

HIGH-RESOLUTION ACOUSTIC ARRAYS USING OPTIMUM SYMMETRICAL-NUMBER-SYSTEM PROCESSING

David Jenn, Phillip Pace, and John P. Powers

Department of Electrical and Computer Engineering
Naval Postgraduate School
Monterey CA 93943-5121
email: jpowers@nps.navy.mil

Introduction

Acoustic arrays can be used for imaging or direction finding. A critical measure of the array's capability is its resolution; here, we will be concerned with the angular resolution of the array, that is, its ability to measure the angular bearing of the target from the array axis. The optimum symmetrical number system (OSNS) can be used to design a simple interferometric acoustic array and to process the data from that array to achieve high resolution angle-of-arrival information. Small angular resolutions may be obtained from a few elements that are spaced a few to several wavelengths apart from each other. The OSNS scheme is based on decomposing the acoustic spatial filtering operation into parallel sub-operations that are each simpler to perform. The results from the parallel operations are combined into an overall high-resolution result. The approach that we use is similar to the approach used to design an RF direction-finding system based on the same concepts [1–5].

Figure 1 indicates the array geometry. Three array elements are indicated (i.e., there are two interferometers); their spacing is determined (from the technique described below) to be 1.50λ and 2.75λ from the end element, where λ is the nominal wavelength of the source. (More array elements may be added, if desired, and different spacings can be prescribed if the element spacings cannot be physically realized.) The angle of arrival, ϕ , is measured from the perpendicular to the array, as shown, and spans a range between -90° and $+90^\circ$. The array elements are receivers that are omnidirectional in the right half-plane. The spacing of the elements and the processing of the signals from them depends on the principles of the optimum symmetrical number system; we now offer a short review of those principles before describing the system design.

Review of Optimum Symmetrical Number System (OSNS)

We begin by choosing N pairwise relatively prime integers (i.e., numbers taken in pairs that contain no common divisor other than 1); these N integers constitute the *moduli* of system, m_1, m_2, \dots, m_N . (For a simple illustration, we choose $N = 2$ with $m_1 = 3$ and $m_2 = 4$.) For each modulus, m_i , we can generate the sequence,

$$x_m = [0, 1, 2, \dots, m_i - 1, m_i - 1, \dots, 2, 1, 0, 0, 1, \dots] . \quad (1)$$

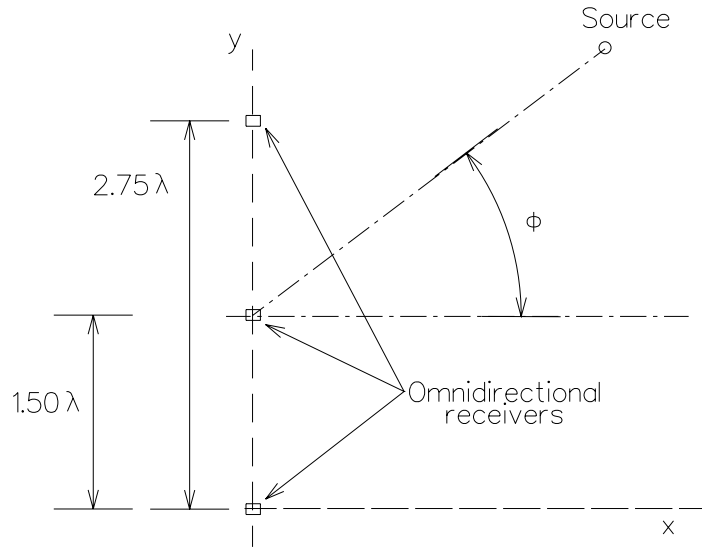


Figure 1: Array geometry.

Index	0	1	2	3	4	5	6	7	8	9	10	11	12
$m_1 = 3$	0	1	2	2	1	0	0	1	2	2	1	0	0
$m_2 = 4$	0	1	2	3	3	2	1	0	0	1	2	3	3

Table 1: Sequences formed from members of two-moduli OSNS ($m_1 = 3$ and $m_2 = 4$).

Table 1 shows the two sequences for our example.

We can consider the index value (i.e., the top row of the table) as an ever-increasing input signal. We note that the values for any particular modulus “fold” as the index continuously increases. In the $m_1 = 3$ row of Table 1, the sequence rise to a maximum of two, then falls back to zero, and then rises to two again. This pattern repeats every six values as the index (the top row of the table) continues to increase. The other row follows the pattern of rising and falling but with different maximum values and, hence, different periods. The $m_2 = 4$ row reaches a maximum of three and has a period of eight. From this we deduce that the sequence period is $2m_i$ and reaches a maximum value of $m_i - 1$. (This folding is reminiscent of the folding of a continuously varying phase, every 2π radians.)

As we count up, we note that no column of values is duplicated until we get to an index of 12 (that duplicates the index 11 column). Hence, the unambiguous dynamic range for our example is 12 (i.e., there are 12 unambiguous states before repetition begins. This value of *dynamic range*, M , is found from $M = m_1 \cdot m_2 \cdots m_N = \prod_{i=1}^N m_i$. For our example, this would be $M = 3 \cdot 4 = 12$ levels.

Figure 2a illustrates the transfer function of the folding circuit that is used to convert the wide dynamic range of the input signal into a small dynamic range output signal. Parallel folding circuits with differing periodicities remove the ambiguity of the single circuit. The folding transfer functions do not need to be linear; they can be nonlinear. Similarly they can have both positive and/or negative values and can extend into negative values of the input function. Examples of folding circuits include phase detectors (mixer followed by a lowpass filter) and Mach-Zehnder electro-optic modulators.

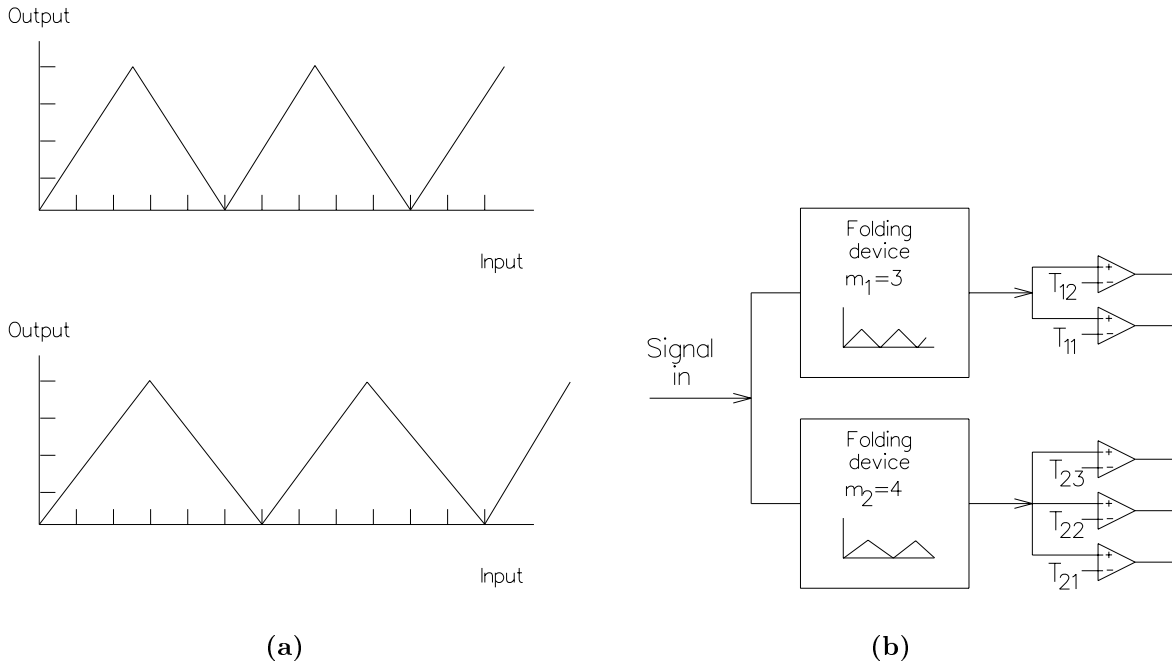


Figure 2: (a) Transfer function of typical folding circuits and (b) folding circuits followed by array of comparators functioning as counting circuits.

Figure 2b shows the folding circuits followed by a bank of comparators. The comparators indicate the range of the corresponding folding-circuit output voltage as a “thermometer” code (i.e., the comparators successively turn on and then off as the input signal increases). Combining the comparator outputs in a logic-gate array allows the user to determine a digital representation of the input value. There are $m_i - 1$ comparators for each channel, each with a different threshold voltage. The threshold voltage T_{ij} for the j -th comparator of the i -th channel is found by dividing the input signal dynamic range into M equal segments and using the transfer function to find the corresponding output value, which is the desired threshold value.

Direction-finding System Concept

Our simple two-modulus example produced only 12 quantization levels, too few for practical use. If we choose our moduli as $m_1 = 6$ and $m_2 = 11$, we will obtain 66 levels, a value with more utility. For each modulus, the periodic sequence described above can be constructed. These sequences have periods of $2m_i$ (i.e., 12 and 22, for our example) and the combination of all sequences extends unambiguously for M values where $M = m_1 m_2 \dots m_N = 6 \cdot 11 = 66$, in our example).

The spacings of the N array elements (measured from a base element) are determined by $d_i = M\lambda/4m_i$ where λ is wavelength of the source [5]. For our conceptual system, the element spacings from the base element are 2.75λ and 1.5λ .

The signal processing of the system (shown in Fig. 3) measures the phase of the i -th element relative to the base element. The phase detectors consist of a mixer and a low-pass filter and produce a (normalized) output voltage of $v_i = \cos(2d_i \sin \phi/\lambda)$ where ϕ is the angle of arrival with values between -90° and $+90^\circ$. The phase-detector voltage is a periodic waveform when plotted against $\sin \phi$. While the voltage out of a *single* phase detector has too many ambiguities to measure the exact phase, the voltages out of *multiple* phase detectors, each with a different period when plotted against $\sin \phi$, can be used to resolve the ambiguities and produce a more exact measurement. In

particular, the range of $\sin \phi$ from -1 to $+1$ (corresponding to the range of ϕ values of $-\pi/2 \geq \phi \leq +\pi/2$) can be subdivided into M different resolution cells. Hence, the resolution of $\sin \phi$ is $2/M = 2/(m_1 m_2 \cdots m_N)$. For our example, this value would be $2/66 = 0.030$. Each resolution cell for $\sin \phi$ can then be transformed into a (nonuniform) resolution cell for ϕ .

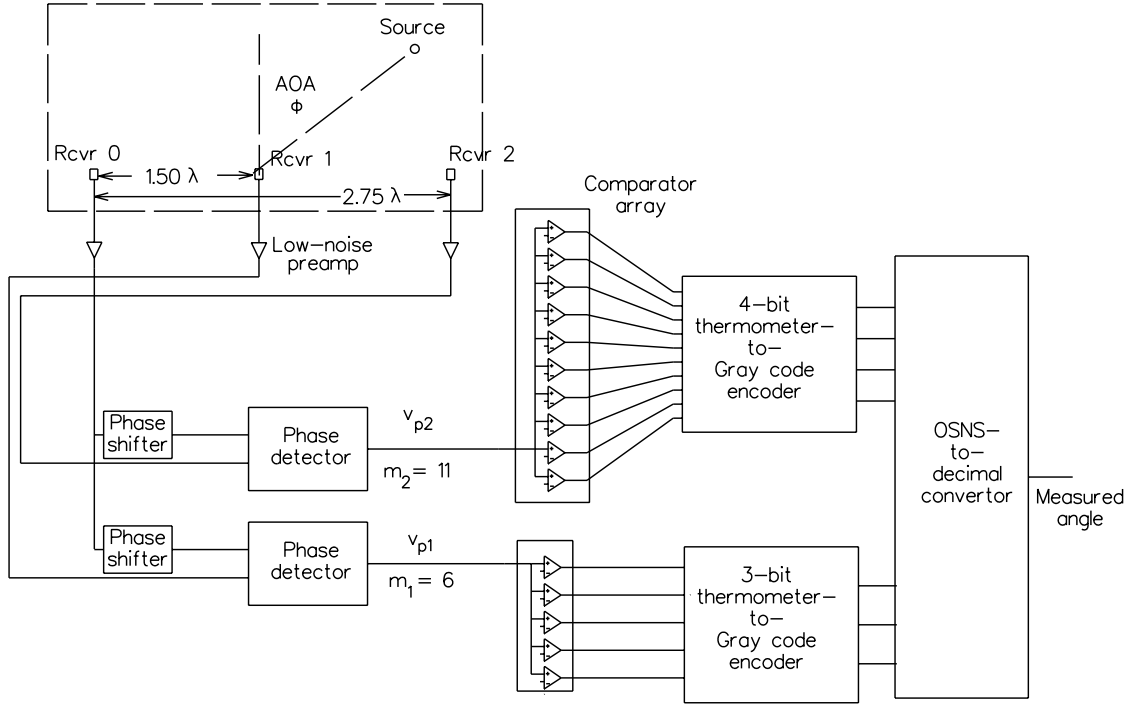


Figure 3: Block diagram of signal processing.

The signal processing required to perform the calculation of the angle of arrival consists of phase detectors feeding a bank of $m_i - 1$ comparators. (For our example, there are 5 and 10 comparators in the two comparator banks.) The threshold voltages of each comparator are set in accordance with the OSNS theory with output of each comparator bank being a thermometer code representing the value of the input in terms of the corresponding OSNS sequence. A digital processing circuit, consisting of an EPROM or an ASIC, converts the thermometer-code output of each comparator bank into a Gray-code output and then combines all of the Gray-code outputs into the high-resolution decimal representation of the angle of arrival (AoA).

The threshold voltages of the comparators are found as follows. We know that there are $m_i - 1$ thresholds to find for a given modulus, m_i . In addition, the range of $\sin \phi$ is divided up into M even increments of size, $\Delta(\sin \phi) = (1 - (-1))/M = 2/M$ (where we recognize that the extreme values of $\sin \phi$ are 1 and -1). For our example, we are seeking five threshold values for $m_1 = 6$ and ten threshold values for $m_2 = 11$. The value of the increments of $\sin \phi$ is 0.0303, as described, and, so, the values of $(\sin \phi)_j$ at each increment are $-1 + 1(0.0303), -1 + 2(0.0303), -1 + 3(0.0303), \dots, -1 + M(0.0303) = +1$. For $m_1 = 6$, we know that the phase-detector output voltage, v_{p1} , will be

$$v_{p1} = \cos \left(\frac{2\pi d_1}{\lambda} \sin \phi \right) = \cos (5.5\pi \sin \phi) , \quad (2)$$

where $d_1 = M\lambda/4m_1 = 2.75\lambda$.

Similarly, for $m_2 = 11$, we find that the phase-detector output voltage, v_{p2} , will be

$$v_{p2} = \cos\left(\frac{2\pi d_2}{\lambda} \sin \phi\right) = \cos(3\pi \sin \phi), \quad (3)$$

where $d_2 = M\lambda/4m_2 = 1.50\lambda$. Table 2 shows the values of $(\sin \phi)_j$ for the first eleven increments and the corresponding values of v_{p1} ($m_1 = 6$) and v_{p2} ($m_2 = 11$). Ignoring the repeated values and the values of +1 and -1, we find the five required threshold values for $m_1 = 6$ to be -0.5, -0.866, 0, 0.5, and 0.866. Similarly, we find the ten threshold values for $m_2 = 11$ as -0.959, -0.841, -0.655, -0.415, -0.1423, 0.1423, 0.415, 0.655, 0.8141, and 0.959. The computed threshold values are also valid if one converts each value of $\sin \phi$ into the corresponding values of ϕ .

Figures 4a and b show the phase detector voltage (normalized) for the $m_1 = 6$ case plotted against $\sin \phi$ and ϕ , respectively. Superimposed on the plots are the five thresholds of the corresponding comparators. Similarly, Figures 4c and d show the normalized voltages for the $m_2 = 11$ case. The corresponding threshold voltages are also superimposed on the plots.

The predicted resolution of the angle-of-arrival is shown in Fig. 5a. The quantity, $\sin \phi$, is evenly divided into M resolution cells, resulting in a nonuniform division of ϕ that is evident in part (b) of the figure. The errors in sampling the phase (deviations from the ideal straight-line plot) are also shown in the figure. The errors in the measurement of $\sin \phi$ are uniform at 0.0303 over the entire range of values. The errors in ϕ are 1.73° (0.0303 radians) for small values of ϕ (broadside) and increase to a maximum error of 14.25° (0.249 radians) for ϕ equal to $\pm 90^\circ$ (end-fire direction).

Summary

We have presented the concept of designing an acoustic array and its signal processing based on the properties of the Optimum Symmetrical Number System (OSNS). The folding properties of the OSNS can be applied to the folding properties of the electronic phase detectors in the array processing system. Table 3 summarizes the relations between the OSNS assumptions and the array system properties. The number of moduli, N , determines the number of elements ($N + 1$) and the number of processing channels. It also contributes to the total number of comparators required. The product of the

j	$(\sin \phi)_j$	v_{p1}	v_{p2}
1	-0.970	0.5	-0.959
2	-0.939	-0.866	-0.841
3	-0.909	-1	-0.655
4	-0.879	-0.866	-0.415
5	-0.848	-0.5	-0.1423
6	-0.818	0	0.1423
7	-0.788	0.5	0.415
8	-0.757	0.866	0.655
9	-0.727	1.0	0.8141
10	-0.697	0.866	0.959
11	-0.667	0.50	1

Table 2: Computed values of $(\sin \phi)_j$ and the corresponding values of phase-detector voltage, v_{p1} for $m_1 = 6$ and v_{p2} for $m_2 = 6$. These voltage values represent the thresholds of the comparators.

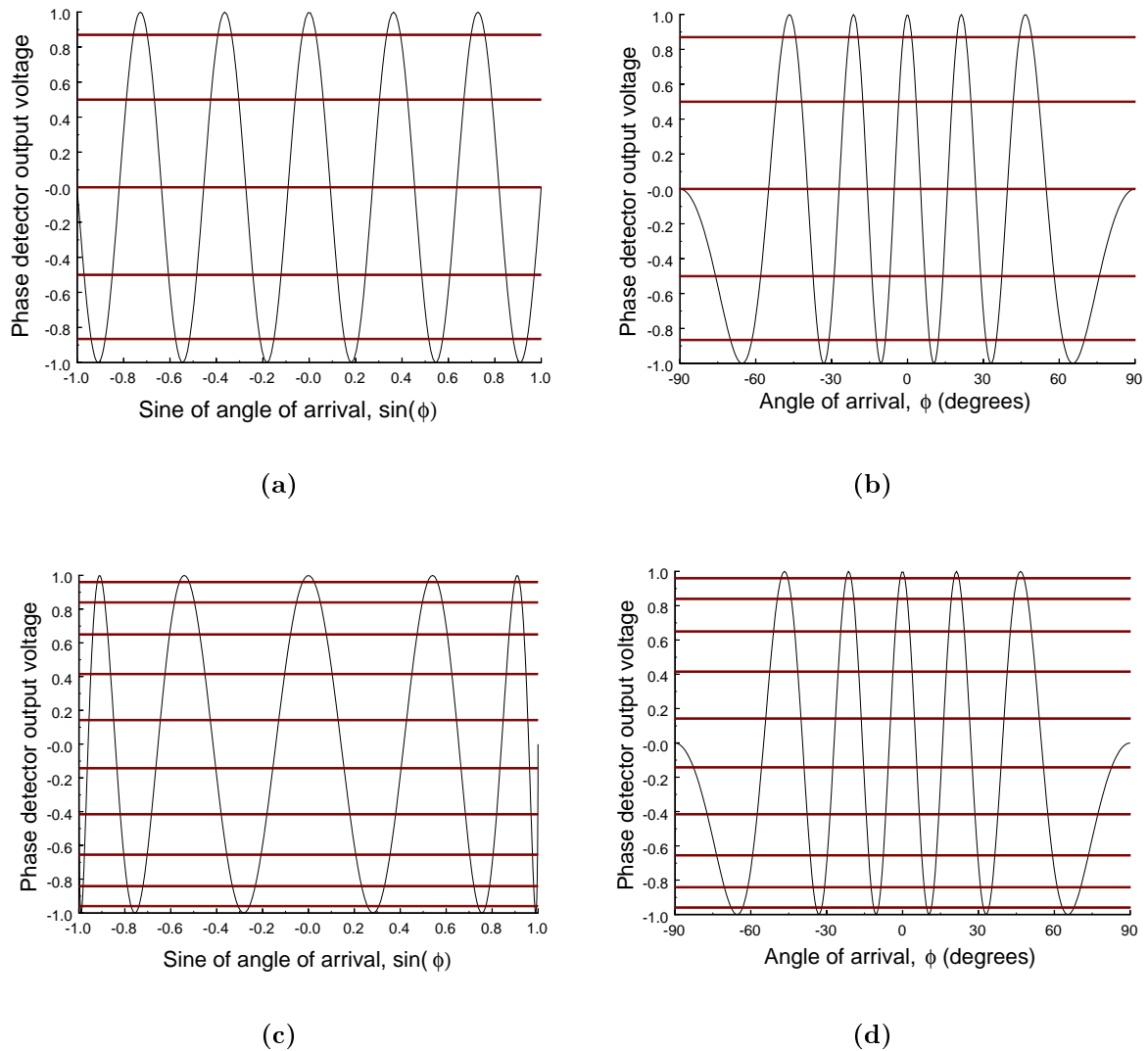
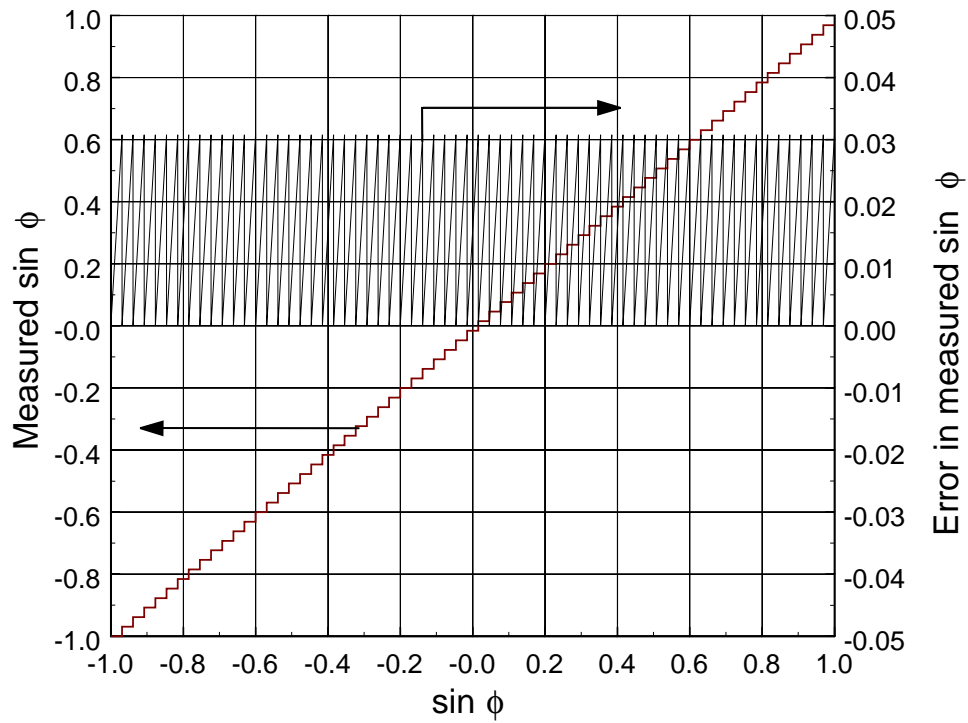


Figure 4: (a) Normalized response of phase detector vs. the sine of the angle of arrival for $m = 6$, (b) normalized response of phase detector vs. the angle of arrival for $m = 6$, (c) normalized response of phase detector vs. the angle of arrival for $m = 11$, and (d) normalized response of phase detector vs. the angle of arrival for $m = 11$. Threshold voltages for the corresponding comparator banks are shown as horizontal lines.

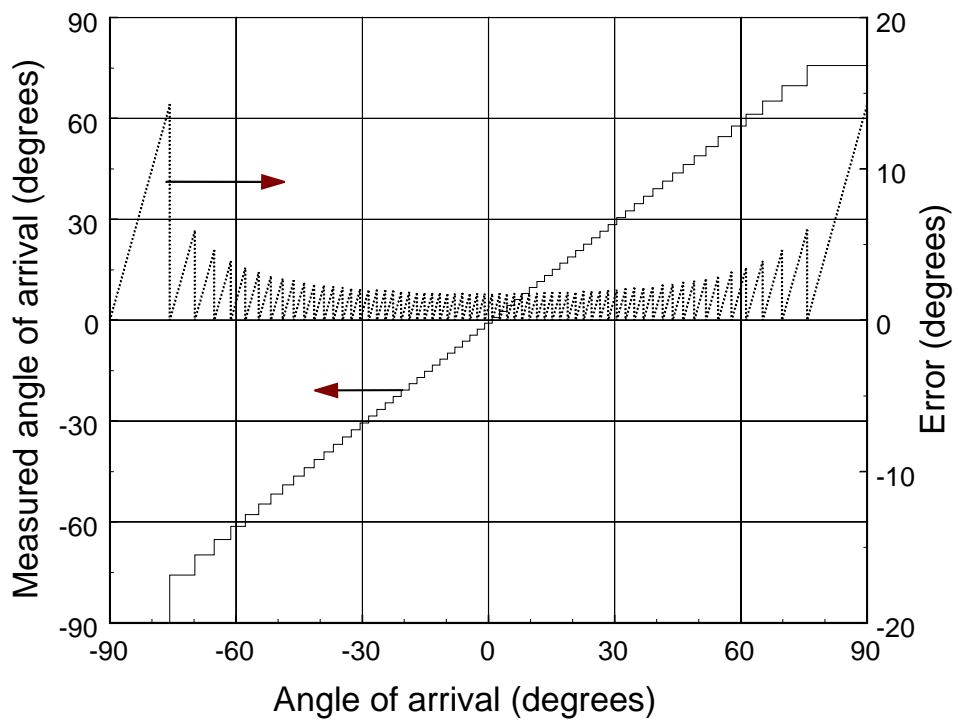
moduli determines the dynamic range of the system, M . This property determines the element spacing and the angular resolution. Generally, for a given resolution, one can tradeoff the overall length of the array against the number of channels (and the number of comparators).

Acknowledgments

The authors wish to thank Prof. David Styer of the University of Cincinnati for his insight into the symmetrical number system and our thesis students for their excellent work on this project. The authors also wish to acknowledge funding by the Department of Defense through the Naval Postgraduate School's Center for Reconnaissance Research and partial support from the NPS Direct-Funded Research Program.



(a)



(b)

Figure 5: Simulated angle-of-arrival results and error for (a) $\sin \phi$ and (b) ϕ .

Property	Value
Moduli	m_1, m_2, \dots, m_N
Number of processing channels	N
Dynamic range	$M = \prod_{i=1}^N m_i$
Number of transducers	$N + 1$
Element spacing (from end)	$d_i = M\lambda/4m_i \quad (i = 1 \dots N)$
Resolution of $\sin \phi$	$2/M$
Resolution of ϕ (degrees)	$\sim 180/M$ (for small ϕ)
Number of comparators for i -th channel	$m_i - 1$
Total number of comparators	$\sum_{i=1}^N (m_i - 1)$

Table 3: Summary of system properties.

References

- [1] L. E. M. Rodrigues, "High-resolution residue antenna architectures for wideband direction finding," Master's thesis, Naval Postgraduate School, June 1996.
- [2] P. Papandrea, "Design and prototype development of an optimum symmetrical number system direction finding array," Master's thesis, Naval Postgraduate School, March 1997.
- [3] D. Jenn, P. Pace, T. Hatziathanasiou, and R. Vitale, "Symmetrical number system phase sampled DF antenna architectures," in *1998 IEEE AP-S International Symposium and URSI North American Radio Science Meeting*, 1998.
- [4] D. Jenn, P. Pace, T. Hatziathanasiou, and R. Vitale, "High resolution wideband direction finding arrays based on optimum symmetrical number system encoding," *Electronics Letters*, vol. 34, no. 11, pp. 1062–1064, 1998.
- [5] T. N. Hatziathanasiou, "Optimum symmetrical number system phase sampled direction finding antenna architectures," Master's thesis, Naval Postgraduate School, June 1998.